Journal of the European Ceramic Society 46 (2026) 118276

Contents lists available at ScienceDirect

Journal of the European Ceramic Society

journal homepage: www.elsevier.com/locate/jeurceramsoc

Strength recovery and degradation behaviors in Al_2O_3-based self-healing ceramics with vanadium carbide additives

Taro Oshiumi [a,b], Toshio Osada [c,d,*], Masahiro Goto [e], Toru Hara [d]

[a] Graduate School of Engineering, Yokohama National University, Tokiwadai 79-5, Hodogaya-ku, Yokohama, Kanagawa 240-8501, Japan
[b] Engineering and Development Departure, Okegawa works, Proterial, LTD., kamihideya 1230, Okegawa, Saitama 363-8510, Japan
[c] Faculty of Engineering, Yokohama National University, Tokiwadai 79-5, Hodogaya-ku, Yokohama, Kanagawa 240-8501, Japan
[d] Research Center for Structural Materials, National Institute for Materials Science, Sengen 1-2-1, Tsukuba, Ibaraki 305-0047, Japan
[e] Research Center for Materials Nanoarchitectonics (MANA), National Institute for Materials Science, Sengen 1-2-1, Tsukuba, Ibaraki 305-0047, Japan

ARTICLE INFO

Keywords:
Al_2O_3–vanadium carbide composite ceramic
Al_2O–SiC–vanadium carbide composite ceramic
Self-healing
Healing agent
Healing activator

ABSTRACT

Ceramic bearings possess superior thermal and mechanical properties but are prone to crack formation and lubricant degradation at high temperatures, driving the development of self-healing ceramics to improve their reliability and lifespan. This study investigates the high-temperature self-healing behavior of surface cracks in Al_2O_3-containing vanadium carbide (VC) particles and Al_2O_3 pre-incorporated with both SiC and VC particles as healing agents. Bending tests show that the required healing time for reaching the strength of 500 MPa in Al_2O_3 containing both VC and SiC achieves approximately 1/6000 times shorter than that in Al_2O_3-SiC composites without VC addition and significantly shorter than that of VC-added Al_2O_3. Excessive internal oxidation of pre-incorporated submicron- to micron-sized VC induces pore formation, reducing strength and hindering full-strength recovery. Formation of a SiO_2 protective layer against SiC oxidation mitigates pore formation. These findings provide a basis for designing ceramics capable of rapid, low-temperature self-healing without pore generation.

1. Introduction

Ceramic bearings, including metal–ceramic hybrid bearings, have been developed and used in applications such as turbine engines [1,2], turbochargers [3], and spindles [3], because ceramics provide superior heat resistance, specific strength, stiffness, abrasion resistance, and corrosion resistance compared with those of metals. However, ceramics are sensitive to defects, and even minute cracks can reduce the overall robustness of products [4]. Furthermore, in the extremely high-temperature range of bearing-operating environments, especially between 400 and 800 °C, both commercial oil-based and solid lubricants deteriorate due to oxidation, resulting in the degradation of hydrodynamic lubrication and interlayer sliding, respectively [5,6]. Consequently, this decline in the lubricant performance increases the frequency of surface-defect initiation caused by direct contact between sliding surfaces, thereby shortening the lifespan of ceramic bearings.

The oxidation-induced self-healing of surface cracks is considered a promising approach for improving the reliability and extending the lifetime of ceramic products [7–25]. In particular, in bearings, repeated contact and frictional stresses on the raceway surface induce the formation of minute surface cracks, which can develop into large-scale flaking (rolling fatigue [26,27]). Therefore, the self-healing of surface cracks represents a key strategy for enhancing reliability. A pioneering study on oxidation-induced self-healing ceramics was conducted by Ando et al. [10], who demonstrated that Al_2O_3 containing 30 vol% SiC as a healing agent achieved full-strength recovery at 1300 °C for 1 h through the high-temperature oxidation of SiC, as described by the following chemical reaction:

$$SiC(s) + 3/2O_2(g) = SiO_2(s) + CO(g) \quad (1)$$

Osada et al. [12] further revealed that the healing mechanism of Al_2O_3–SiC composites, similar to bone healing, can be divided into three stages: (1) initiation of high-temperature oxidation of SiC, as shown in Eq. (1) (inflammation stage); (2) reaction of the formed SiO_2 with the

Abbreviations: 3D, three-dimensional; ASiCVC, Al_2O_3–20vol% SiC–10vol% vanadium carbide; AVC, Al_2O_3–10vol% vanadium carbide composites; BSE, back-scattered electron; EDS, energy-dispersive X-ray spectroscopy; SEM, scanning electron microscopy; VC, vanadium carbide; XRD, X-ray diffraction.

* Corresponding author at: Research Center for Structural Materials, National Institute for Materials Science, Sengen 1-2-1, Tsukuba, Ibaraki 305-0047, Japan
E-mail address: OSADA.Toshio@nims.go.jp (T. Osada).

https://doi.org/10.1016/j.jeurceramsoc.2026.118276
Received 17 November 2025; Received in revised form 13 February 2026; Accepted 2 March 2026
Available online 3 March 2026

surrounding Al_2O_3 to produce low-viscosity supercooled melts that completely fill cracks (repair stage); and (3) nucleation and growth of mechanically strong crystals within the supercooled melts (remodeling stage). Furthermore, a novel design approach using a three-dimensional (3D) network of a healing activator was proposed to accelerate the repair and remodeling stages. Consequently, it was demonstrated that Al_2O_3–SiC doped with 1 vol% MnO as a healing activator achieves full-strength recovery at 1000 °C within 1 min. These findings suggest that pre-incorporating suitable combinations of healing agents and activators into the ceramic matrix enables the design of self-healing ceramics capable of repairing surface cracks under various temperature conditions appropriate for specific components. Further, to achieve low temperature healing, various studies have reported using Ti compounds [18–22] and MAX phases [23–25] as healing agents to accelerate inflammation reaction, as well as approaches that utilize external electrical energy [28,29].

Based on the above background, this study focuses on the development of Al_2O_3-based ceramics containing vanadium carbide (VC) particles for bearing applications. VC is considered an attractive self-healing agent because, although its melting point is 2800 °C, it readily oxidizes to V_2O_5 in air above 600 °C, reducing the effective melting point to 680 °C [30,31]. Therefore, even when VC is incorporated into the ceramic base material, the low-viscosity V_2O_5 is expected to efficiently fills crack-gaps during the inflammation and repair stages at lower temperatures than the SiC healing agent, without substantially compromising the overall heat resistance of the system. From this perspective, Al_2O_3-based ceramics containing VC are anticipated to exhibit self-healing behavior within the operating temperature range of bearings.

In addition, V_2O_5 formed from VC oxidation serves not only as a healing activator with viscosity modifier that facilitates the repair and remodeling stages, similar to the role of MnO [12], but also potentially acts as an oxidizer during the inflammation stage in Al_2O_3–SiC self-healing. Molten V_2O_5 has been reported to exhibit good wettability with SiC and promote its oxidation above 670 °C [32]. Thus, in Al_2O_3-based self-healing ceramics containing both SiC and VC particles, the V_2O_5 formed from VC oxidation could accelerate the inflammation reaction of SiC as a healing agent with an oxidizer. Subsequently, similar to the healing activator MnO, V_2O_5 can decrease the viscosity of the supercooled melts in the SiO_2–Al_2O_3 system. Preliminary calculations using commercial thermodynamic software (FactSage) estimate that the glass-transition temperature (T_g) of the SiO_2–Al_2O_3–V_2O_5 ternary system, which marks the lowest temperature at which the repair stage can begin, is below 300 °C. This is approximately 650 °C lower than that of the SiO_2–Al_2O_3 system (T_g = 943 °C) and 180 °C lower than that of the SiO_2–Al_2O_3–MnO system (T_g = 479 °C) [12]. These results suggest that V_2O_5 has the potential to improve the strength-recovery rate of Al_2O_3–SiC composites and lower the healing temperature compared with the SiO_2–Al_2O_3–MnO system.

More importantly, the formed V_2O_5 can reduce the friction coefficient by acting as a self-lubricant [33–38]. Broniszewski et al. has been reported that addition of 2.5% V to Al_2O_3 reduced the friction coefficient by ~30% at 500 °C and by ~50% at 800 °C, and reduced the wear coefficient by ~80% at both temperatures, because of the V_2O_5 formed on contact surface [38]. Its layered crystal structure of V_2O_5 [33], similar to that of graphite, facilitates interlayer sliding. In addition, when V_2O_5 is liquefied at high temperatures or under load, its viscosity, measured below 60 Pa·s [34] and comparable to that of engine oil, can provide hydrodynamic lubrication. Therefore, incorporating VC shows promise for designing ceramic bearings capable of self-lubrication, avoiding lubricant degradation, and preventing rolling failure under operating conditions. Although numerical studies have examined the self-lubricating properties of vanadium oxides [35–38], no studies have attempted to design ceramics that combine self-lubrication with reduced healing temperatures for practical bearing applications.

To develop high-temperature ceramic bearings with both self-healing and self-lubricating abilities, we investigated the self-crack-healing and strength-recovery behaviors of two types of Al_2O_3-based composites containing VC as both the healing agent and activator. The composites fabricated in this study were Al_2O_3–10 vol% VC (AVC) and Al_2O_3–20 vol% SiC–10 vol% VC (ASiCVC), both of which contained 10 vol% VC particles. In previous study by Osada et al. [12], they proposed a self-healing ceramics containing trace amounts (less than 1.0 vol %) of MnO, an oxide, as a 3D network of healing activator. In contrast, in this study, we aimed to develop composites with self-lubricating as a future goal by adding 10 vol% VC as a carbide rather than as an oxide, so that a sufficient amount of oxide would form on the surface as a lubricating layer during high-temperature oxidation. Furthermore, note that the VC particles are uniformly dispersed as a healing agent, rather than a three-dimensional network of healing activator in the composites. Here, the volume fraction of SiC and VC in ASiCVC was set to a total of 30 vol % or less to prevent inhomogeneous particle mixing and agglomeration. In the AVC composites, the performance of VC as a healing agent was evaluated by examining the strength-recovery behavior and microstructural evolution of the healed regions. In the ASiCVC composites, the effect of the formed vanadium oxide as a healing activator on the strength recovery of the Al_2O_3–SiC composites was also assessed. Furthermore, the self-healing mechanisms of surface cracks in composites containing both SiC and VC were analyzed by comparing the strength-recovery behavior at room temperature and crack-gap filling behavior at the surface and subsurface. While this study focuses on recovery behavior of the room-temperature strength, findings here are an important step prior to evaluating the high-temperature strength recovery behavior and lubrication properties in the 400–800°C range, which corresponds to bearing operating conditions.

2. Materials and methods

2.1. Materials

Raw powders of α-Al_2O_3 (average diameter 0.4 μm, purity 99.99%, AKP-20, Sumitomo Chemical Co., Ltd., Tokyo, Japan), β-SiC (average diameter 0.5 μm, BF17, H. C. Starck, UK), and VC (average diameter 1.7 μm, purity 97%, Japan New Metals, Japan) were used in this study. Suspensions of AVC and ASiCVC were weighed and ball-milled in isopropanol for 24 h using F5 alumina balls and milling pots. The mixtures were then dried on a hot plate at 200 °C for 2 h and sieved through a 500-μm mesh to obtain a dry powder mixture. Rectangular plates with dimensions of 40 mm × 40 mm × 5 mm were subsequently fabricated by hot-pressing in a furnace (High-multi15000, Fuji Dempa, Japan). The hot-pressing of AVC and ASiCVC was conducted under an Ar atmosphere at 40 MPa for 1 h, at temperatures of 1600 and 1750 °C, respectively. For both materials, the heating and cooling rates were 10 and 5 °C/min, respectively. The relative densities of the sintered AVC and ASiCVC plates were measured by the Archimedes' method, using theoritical densities of 4.15 and 4.00 g/cm^3, respectively. For comparison, monolithic Al_2O_3 was prepared by hot-pressing α-Al_2O_3 powder under Ar at 1500 °C and 40 MPa for 1 h.

2.2. Self-healing and mechanical tests

The sintered bodies were cut into rectangular bar specimens measuring 40 mm × 4 mm × 3 mm. The edges of the specimens were chamfered at 45° to prevent fracture initiation from edge cracks. The specimen surfaces were polished to a mirror finish, with a surface roughness (R_a) ≤ 0.2 μm, following JIS standards [39], and were designated as smooth specimens. A semi-elliptical surface pre-crack, approximately 110 μm in length ($2c$) and approximately 50 μm in depth (a), was introduced at the center of each smooth specimen surface by Vickers indentation using a load of 19.6 N (ARS-F, Future Tech, Japan). The aspect ratio of the cracks (a / c) was approximately 0.9, where a and c represent the crack depth and half-length, respectively.

Here we note that depth of pre-crack could be few times larger than that observed during the actual rolling fatigue (usually, < 10 μm in depth corresponding to few times of grain size [27]). However, in this study, we select size with surface length of 110 μm and depth of 50 μm as a standard crack size for a conservative evaluation of self-healing of crack, because of the two main reasons; difficulty to reproduce a small crack with depth of below 10 μm by Vickers indentation method; importance to compared to strength recovery behaviour with previous study. As-cracked specimens were healed in air at 700–1000 °C for 10 min to 100 h using an electric furnace (1500Plus, Yamato Scientific Co., Ltd., Tokyo, Japan). The healed samples were tested in three-point bending at room temperature with a span length of 30 mm. The crosshead speed was 0.5 mm/min, following the JIS standard [39].

2.3. Microstructural characterization

The initial microstructures of AVC and ASiCVC were examined using scanning electron microscopy (SEM) equipped with an energy-dispersive X-ray spectroscopy (EDS) detector (JEM-7001F, JEOL, Tokyo, Japan). The average atomic number of VC is approximately 14.5, which is approximately 1.5 times higher than that of Al_2O_3 and SiC, making VC particles easily distinguishable in backscattered electron (BSE) images. The average size of the VC particles (d_{VC}) was determined from BSE images containing more than 800 numbers of VC, as the area-equivalent diameter using ImageJ (NIH, Bethesda, MD, USA).

The bulk surfaces before and after heat treatment were examined using an optical microscope (VHX-6000, KEYENCE, Osaka, Japan) and a surface recorder (SE800, KOSAKA Lab., Tokyo, Japan). The R_a was determined from nine measurements, three locations on each of three

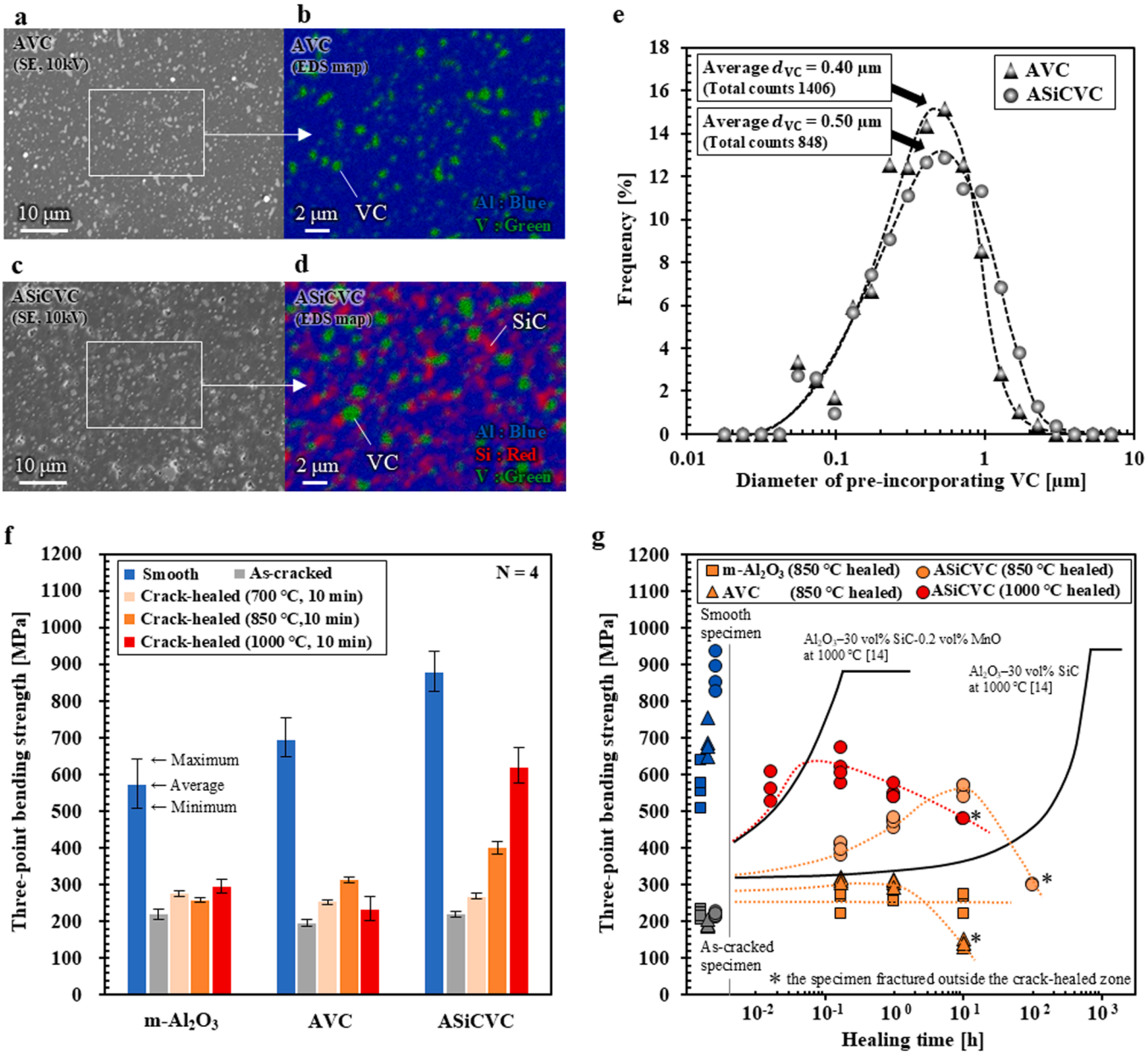

Fig. 1. Initial microstructures and strength-recovery behaviors by self-healing in Al_2O_3–10 vol% vanadium carbide (VC) composites (AVC) and Al_2O_3–20 vol% SiC–10 vol% VC (ASiCVC). (a) Secondary electron (SE) image of sintered AVC obtained at accelerating voltage of 10 kV. (b) Energy-dispersive X-ray spectroscopy (EDS) mapping image of sintered AVC. (c) SE image of sintered ASiCVC obtained at accelerating voltage of 10 kV. (d) EDS mapping image of sintered ASiCVC. (e) Distribution of pre-incorporated VC. (f) Effect of the healing temperature on the strength-recovery behavior (healing temperature: 700–1000 °C, healing time: 10 min). (g) Effect of the healing time on the strength-recovery behavior (healing temperature: 850–1000 °C, healing time: 10 min to 100 h).

samples ($N = 9$), and is presented as average R_a with standard deviation. Moreover, the crystal structures of the various phases on the bulk surfaces were identified by X-ray diffraction (XRD, X'Pert PRO, PANalytical, Almelo, Nederland) using Cu$K\alpha$ radiation generated at 45 kV and 40 mA.

To investigate the crack-healing behavior, the healed cracks in AVC and ASiCVC were examined using a focused ion beam (FIB)–SEM system (Scios 2, Thermo Fisher Scientific, Massachusetts, USA). Thin plates measuring 10 μm × 10 μm × 0.1 μm were extracted using the same instrument. The thinned plates were then analyzed with a scanning transmission electron microscope (STEM, JEM-2800, JEOL, Tokyo, Japan) equipped with dual 100 mm^2 EDS detectors at an accelerating voltage of 200 kV.

The fractured surfaces of the samples were examined using optical microscopy (VHX-6000, KEYENCE) and SEM equipped with EDS (JEM-7001F, JEOL). Here, the internal oxidation depth was also measured as the average of the measurements taken at three locations: both edges and the center of the fracture surface of specimens healed at 850°C and 1000°C for 10 min to 100 h. For the AVC with large internal oxidation and ASiCVC with limited internal oxidation were measured by optical microscopy and SEM, respectively.

3. Results

3.1. Initial microstructures and strength-recovery behaviors

Fig. 1 shows the initial microstructures and strength-recovery behaviors of AVC and ASiCVC during self-healing. Secondary electron (SE) images of the sintered AVC and ASiCVC confirm the formation of dense bodies (Fig. 1a and 1c). Archimedes' method indicated that the relative densities of AVC and ASiCVC were greater than 99% and 98% of the theoretical densities, respectively. Elemental analysis revealed that the pre-incorporated VC and SiC particles were uniformly dispersed within the Al_2O_3 matrix (Fig. 1b and 1d**)**. The d_{VC} values were measured from BSE images (Fig. 1**e**) as approximately 0.40 and 0.50 μm, based on particle counts of 1406 and 848, respectively, indicating that ball milling reduced the d_{VC} to approximately one-third of its initial value. These results confirm that submicron-to micron-sized VC particles were distributed in both AVC and ASiCVC composites with similar distribution characteristics. Further, here we note that V were distributed as VC homogeneously in initial microstructure, but not localized at grain boundary which act as crack propagated site, as 3D networks of healing activators (MnO) reported by Osada et al. [12], at least SEM-EDS level analysis (Fig. 1b and d).

Fig. 1**f** shows the effects of the healing temperature on the strength-recovery behavior of Al_2O_3, AVC, and ASiCVC. The healing temperatures ranged from 700 to 1000 °C, and the healing time was 10 min. The bar plots represent the average values, and the upper and lower ends of the error bars indicate the maximum and minimum values, respectively, among the four measurements. The strengths of the smooth AVC and ASiCVC specimens were 692 and 878 MPa, respectively, both of which were higher than that of monolithic Al_2O_3, which was 571 MPa. These results suggest that the strength of the smooth specimens increased as the grain size decreased owing to the pinning effect of the added particles. The strengths of the as-cracked specimens of monolithic Al_2O_3, AVC, and ASiCVC specimens were approximately 200 MPa, implying that even a small surface crack with a length of 110 μm significantly reduced the strength. After healing at 700 °C for 10 min, the average strengths of AVC and ASiCVC increased slightly to 260 MPa, with no significant difference in strength recovery compared with monolithic Al_2O_3. The minor strength recovery in monolithic Al_2O_3 was attributed to not self-crack-healing but to the relaxation of tensile residual stresses at the Vickers indentation cracks, as reported by Ando et al. [8]. After healing at 850 °C for 10 min, the average strengths of AVC and ASiCVC increased to approximately 313 and 402 MPa, respectively, slightly and moderately higher than that of monolithic Al_2O_3, which was 257 MPa. These results confirmed that both AVC and ASiCVC composites exhibit self-crack-healing ability above approximately 850 °C. Under the 1000 °C healing condition, the average strengths of the healed AVC and ASiCVC specimens were 232 and 620 MPa, respectively, with only ASiCVC showing significantly superior strength recovery compared with that of monolithic Al_2O_3. Notably, AVC exhibited an unexpected strength degradation under this condition.

To clarify the strength-recovery and degradation behaviors of both composites at high temperatures, the dependence of the healing time on the strength recovery was evaluated, as shown in Fig. 1g. Asterisks indicate specimen that fractured at sites other than the pre-crack. For comparison, the experimental strength-recovery behavior of Al_2O_3–30 vol% SiC-0.2 vol% MnO and Al_2O_3–30 vol% SiC at 1000 °C [12], are also shown in the Fig. 1g as solid lines.

The strength of AVC composites increased slightly with the healing time, reaching 313 MPa after 10 min at 850 °C. Although the strength recovery is limited, it is attributed to crack-gap filling by oxidation products formed from the self-healing reaction of VC particles (as described in 3.2 and 3.3), as evidenced by the slightly higher strength compared with that of Al_2O_3. However, for longer healing durations, the strength decreased significantly. After 10 h, the strength fell below that of Al_2O_3. Nevertheless, the specimens fractured at sites other than the pre-crack, indicating that the cracks were not fully healed and that deterioration occurred owing to VC oxidation, as discussed in 3.4.

The strength of the ASiCVC composites increased markedly with longer healing times, reaching peak values of 567 MPa at 850 °C and 620 MPa at 1000 °C after 10 h and 10 min, respectively. Furthermore, ASiCVC showed superior strength recovery compared with that of AVC. Moreover, the ASiCVC achieve the strength of 500 MPa at 1000 °C for 1 min, whereas the Al_2O_3-30 vol% SiC composites reported to be required approximately 100 h for reaching this level of strength. Notably, the required healing time for reaching the strength of 500 MPa in ASiCVC was 1/6000 times shorter than that in Al_2O_3-SiC composites without VC addition, and comparable to that in Al_2O_3-SiC-MnO composites [12]. The activation of self-healing by VC doping suggests that the formed V_2O_5 may assist in the repair and remodeling stages in Al_2O_3–SiC healing, similar to MnO [12]. However, ASiCVC exhibited unexpected strength degradation, resulting in a lower peak strength than that of the smooth specimens. Thus, although VC doping effectively accelerated strength recovery, ASiCVC did not achieve full-strength restoration.

3.2. Oxidation behaviors on composites surfaces

To analyze the healing and deterioration behaviors, the oxidation and crystallization behaviors of the top surfaces of the specimens were investigated. Fig. 2 shows the oxidation behavior of the bulk surface of AVC. Before self-healing, polishing scratches and the Vickers indentation were visible, with a R_a of approximately 0.09 μm (Fig. 2a). After self-healing, the surface textures of the bulk body changed markedly at all heat-treatment temperatures, and both the scratches and Vickers indentation marks disappeared (Fig. 2b–d). Moreover, increasing the heat-treatment temperature led to a higher R_a in AVC. In particular, heat treatment at 1000 °C caused the formation of bumps and voids, resulting in a R_a of 12.79 μm (Fig. 2d). XRD analysis showed that the Al_2O_3 and VC phases were primarily detected before healing (Fig. 2e), whereas the V_2O_5 phase appeared after healing (Fig. 2f–h). The peak intensities and patterns varied with the heat-treatment temperature. At 700 °C, the XRD pattern exhibited three strong peaks corresponding to V_2O_5 (200), (010), and (400) (Fig. 2f). At 850 °C, a single prominent peak corresponding to V_2O_5 (010) was observed (Fig. 2g). At 1000 °C, no distinct high-intensity peaks were detected (Fig. 2h). Here, the pronounced decrease in the V_2O_5 (010) and (020) peaks at 1000 °C oxidation for AVC is attributed primary to significant increment of the surface roughness and thickness of oxidation layer. The presence of bumps and voids, together with the observation that brown-collared V_2O_5 phase forms a

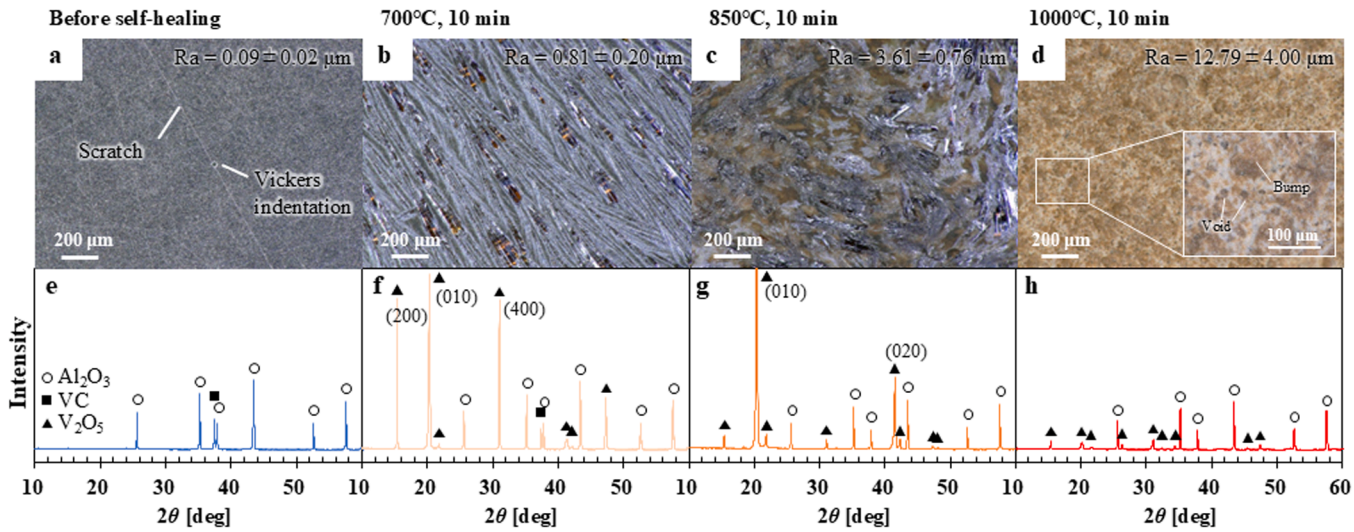

Fig. 2. Oxidation behavior of the bulk surface in AVC. (a–d) Photographs of the bulk surface before and after healing. (e–h) X-ray diffraction patterns before and after healing.

discontinuous pattern, could be resulting in that preferred orientation associated with the sheet-stacking direction of V_2O_5 was disrupted by the increased surface roughness.

Fig. 3 shows the oxidation behavior of the bulk surface of ASiCVC. Before self-healing, polishing scratches and the Vickers indentation were observed, with a R_a of approximately 0.09 μm (Fig. 3a). After self-healing, the surface textures of ASiCVC changed markedly at all heat-treatment temperatures, and the positions of the scratches and Vickers indentations were no longer identifiable (Fig. 3b–d). However, in contrast to the results for AVC, the deterioration of the R_a was limited to less than 1 μm. Bumps and voids were not observed on the surface of ASiCVC after healing at 1000 °C healing, indicating that the addition of SiC effectively suppresses the deterioration of the R_a. According to the XRD results, the main oxide formed was V_2O_5 (Fig. 3e–h). Unlike AVC, the VC (111) and V_2O_5 (010) high-intensity peaks remained even after healing at 1000 °C. In addition, the SiC (111) peak was observed before and after healing, but the SiO_2 peak could not be detected in this measurement, indicating that the amount of SiO_2 crystal phase was lower than that of V_2O_5 on the bulk surface.

Based on the above results, it was confirmed that a significant amount of V_2O_5 formation occurred as expected at heat-treatment temperatures of 700 °C or higher. Even at 700 °C, the surface texture changed drastically, indicating that VC is excellent in terms of the precipitation rate of healing materials, namely vanadium oxides, which are a key factor for a healing agent. Furthermore, the addition of SiC effectively prevented surface deterioration.

3.3. Analysis of structure and compositions at healed cracks

For a more detailed investigation, the structure and composition of the healed Vickers cracks in AVC and ASiCVC, extracted using FIB, were analyzed. Further, it is important to directly analyze the structure of healing materials within the narrow crack gap cracks after healing, since it was reported that the oxidation products within the narrow crack gap could slightly differ from oxide formed on sample surface detected by XRD [12]. Fig. 4 shows SEM and STEM images around a crack in AVC healed at 700 °C for 10 min. The results of the EDS analysis of the healed cracks are summarized in Table 1. As shown in the SEM images of the healed crack before FIB extraction (Fig. 4**a**), typical Vickers indentation cracks, including medial and lateral cracks, were observed. The

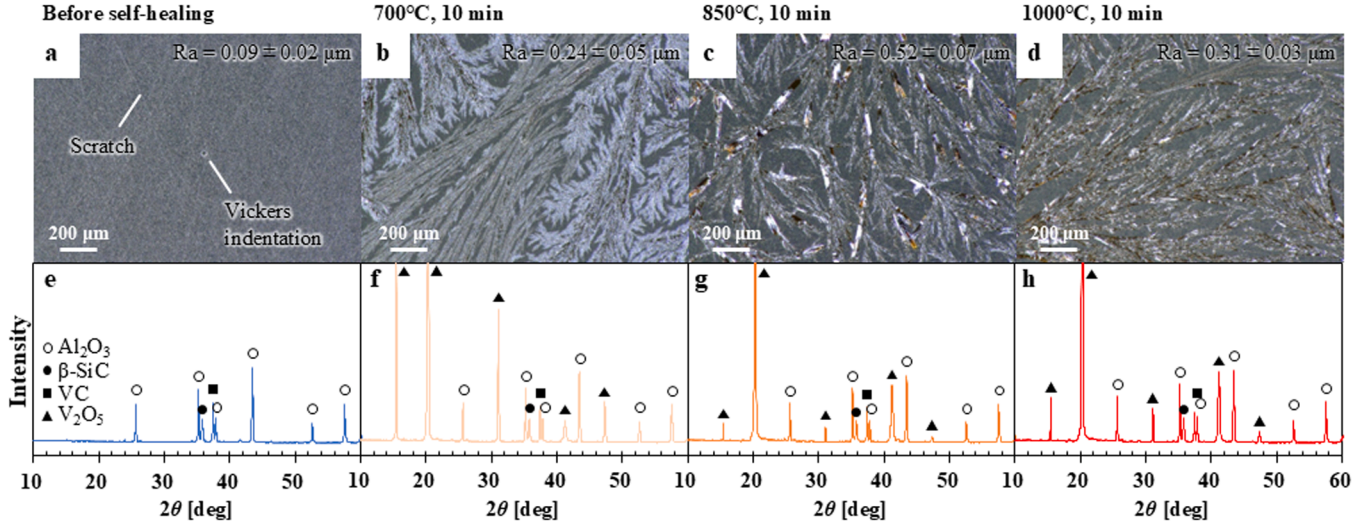

Fig. 3. Oxidation behavior of the bulk surface in ASiCVC. (a–d) Photographs of the bulk surface before and after healing. (e–h) X-ray diffraction patterns before and after healing.

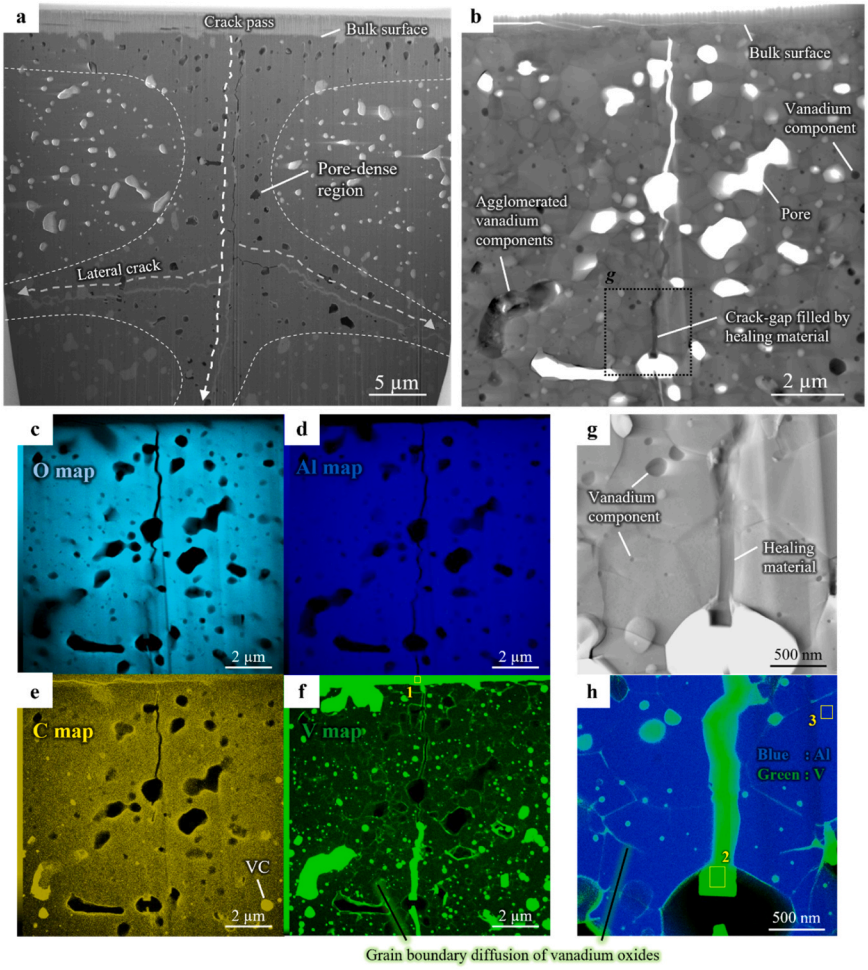

Fig. 4. (a) TEM image of an indentation crack after crack-healing in AVC at 700 °C for 10 min. (b) Bright-field STEM image of the indentation crack after healing. (c–f) Elemental mapping images corresponding to panel (b). (g) High-magnification high-angle annular dark-field STEM image. (h) STEM–energy-dispersive X-ray spectroscopy (EDS) mapping corresponding to panel (g).

Table 1
EDS analysis of the region surrounding the healed crack in AVC.

Area	Element [at%]			
	C	O	Al	V
1	2.13	18.46	2.82	76.60
2	-	28.36	3.34	68.30
3	-	60.29	39.68	0.03

crack-gaps were sufficiently filled by the formed oxide in regions deeper than approximately 20 μm from the surface. Meanwhile, near the bulk surface, where the crack-gaps were larger, the medial crack was only partially filled by oxide. These results suggest that the full or partial filling of crack-gaps contributed to the slight strength recovery observed in Fig. 1**f**. In addition, numerous pores ranging from submicron to micron sizes were identified within approximately 5 μm of both the crack and bulk surfaces (pore-dense region). This indicates that the pores formed due to the disappearance of submicron- to micron-sized VC particles (Fig. 4**a**) after oxidation. Furthermore, the formation of dense pores results in degradation, as shown in Fig. 1**g**.

The STEM-HAADF images and EDS maps for O, Al, C, and V in the region where the crack was partially filled near the bulk surface are shown in Fig. 4b–f. The arrangement of VC particles and pores, as well as their contribution to the self-healing reaction, were confirmed. Within the pore-dense region, micron-sized VC particles disappeared after oxidation, whereas fine submicron-sized VC particles encapsulated within the alumina grains remained, either as oxides (V_xO_y) or partially as VC. EDS mapping revealed that a small amount of V was concentrated at the grain boundaries, alumina/VC interface, and pore surfaces. Furthermore, oxides formed within the crack-gap and on the partially bonded crack surfaces (Fig. 4c–f). Elemental analysis confirmed that VC present on the crack surface, as well as VC near the crack surface, contributed to crack-gap filling during the self-healing reaction. Furthermore, V was supplied to both the crack-gap and bulk surface through outward diffusion along grain boundaries and interfaces. An edge-like oxide was also observed within the filled crack-gap, indicating that the oxide had crystallized. High-magnification STEM combined with EDS analysis revealed that the edge-like oxide contained a small amount of Al_2O_3 (Figs. 4g and 4h, Table 1), suggesting that its melting point is lower than the healing temperature of 700 °C (as discussed in 4.1). Furthermore, the V–Al ratio in the healed regions was similar to that of the bulk surface. XRD analysis confirmed that the bulk surface oxides were mainly composed of crystallized V_2O_5 (Fig. 2). Therefore, the oxides formed in the healed regions of AVC likely crystallized into V_2O_5 as well. It can be concluded that the crack-gap filler consisted of a V–Al–O melt that fully crystallized into a V_2O_5-based material with a weak interlayer during cooling in the self-healing process, indicating that the addition of VC as a healing agent in alumina resulted in limited self-healing performance.

Fig. 5 shows SEM and STEM images around a crack in ASiCVC healed at 1000 °C for 10 min, where the strength reached 675 MPa. The results

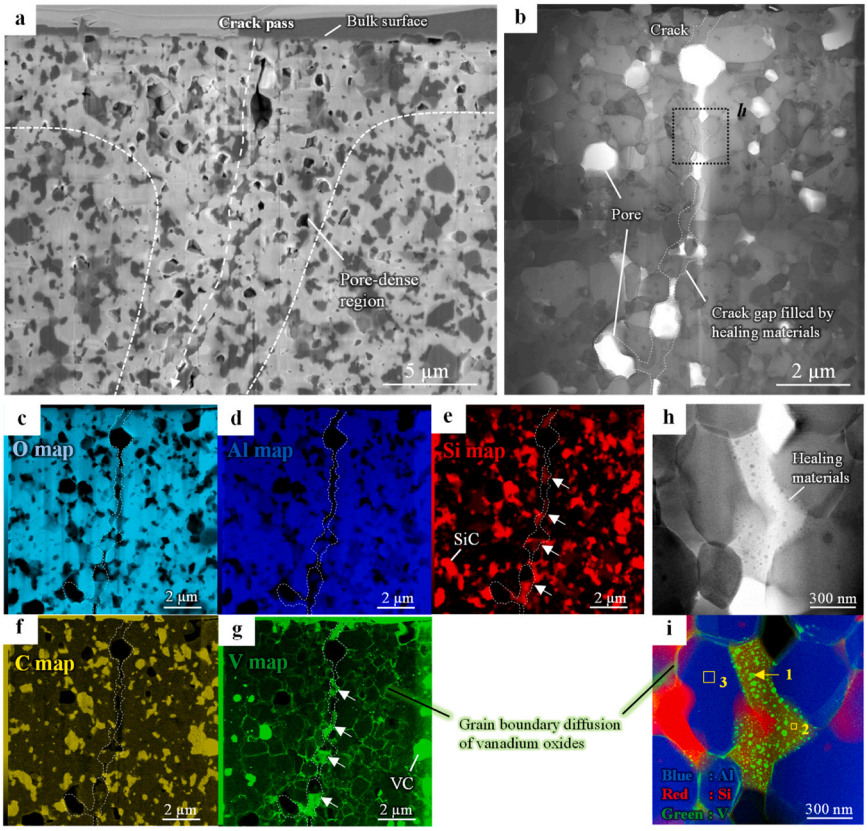

Fig. 5. (a) Scanning electron microscopy image after crack-healing in ASiCVC at 1000 °C for 10 min. (b) Bright-field TEM image of an indentation crack after healing. (c–g) Elemental mapping images corresponding to panel (b). (h) High-magnification high-angle annular dark-field STEM image. (i) STEM-EDS mapping corresponding to panel (h).

of the EDS analysis of the healed region are listed in Table 2. As shown in Fig. 5a, the crack-gap was sufficiently filled with oxides compared with that of AVC, implying that the addition of SiC effectively promotes the formation of filling oxides. A pore-dense region was also observed within approximately 5 μm of both the crack and bulk surfaces, similar to AVC. However, the width of the pore-dense region in ASiCVC was comparable to that in AVC, despite the healing temperature being 300 °C higher (Fig. 4). This suggested that the addition of SiC can help prevent the disappearance of submicron- to micron-sized VC particles.

STEM-HAADF images and EDS maps for Al, O, Si, C, and V in the region where the crack-gap was filled are shown in Fig. 5b–g. The arrangement of both SiC and VC healing agents and their respective contributions to the self-healing reaction were confirmed. EDS mapping images revealed that only the SiC located on the crack surface was oxidized, and the formed oxides sufficiently filled the crack-gap. However, SiC encapsulated within the alumina particles remained stable at high temperatures. Meanwhile, micron-sized VC particles disappeared owing to oxidation, similar to AVC, resulting in the formation of a pore-dense region. However, a relatively small number of fine submicron-sized VC particles encapsulated within the alumina grains remained, either as oxides (V_xO_y) or partially as VC. Furthermore, V was supplied from VC near the crack surface to the crack-gap via outward diffusion, similar to the healing behavior in AVC, as evidenced by small amounts of V concentrated at the grain boundaries, alumina/VC interface, and pore surfaces. As a result of the oxidation of the two healing agents, SiC and VC, the oxides formed within the crack-gap were primarily composed of Si–V–O (Figs. 5**c**, 5**e**, and 5**g**). Further detailed observations by high-resolution STEM and EDS mapping (Figs. 5**h** and 5**i**) clearly suggested that the formed oxide consisted of two phases: a Si-rich matrix phase and V-rich fine precipitates. EDS analysis of areas 1–3 in Table 2 showed that the converted SiO_2:V_2O_5:Al_2O_3 mole ratios in the Si-rich matrix phase and V-rich fine precipitates were approximately 96:2:1 and 86:13:1, respectively. These results indicate that the crack-gap filler was a SiO_2-rich glass phase in which Si–V–Al–O supercooled melts or melts fully crystalized and separated into two phases during the self-healing process (heating and cooling).

The above results revealed that in both AVC and ASiCVC, V diffused to the crack-gap and bulk surface through alumina grain boundaries, which acted as diffusion paths. Interestingly, the V element mapping results within pore-dense region looks like similar structure to the designed 3D network for a healing activator using MnO reported in [12]. However, the V-network obtained after oxidation is totally different from 3D network of MnO-healing activator designed in initial microstructure, and conclude to be a structure as a result of grain boundary diffusion. Note that this also implied that the V_2O_5 formed by rapid oxidation from homogeneously distributed VC particles can accelerate the self-healing similar to 3D network of MnO-healing activator.

Table 2
EDS analysis of the region surrounding the healed crack in ASiCVC.

Area	Element [at%]				
	C	O	Al	Si	V
1	6.04	50.17	0.78	32.92	10.10
2	5.64	50.94	0.86	40.77	1.78
3	3.93	59.83	35.46	0.76	0.01

3.4. Degradation behaviors of surface and strength

Fig. 6 shows the degradation behavior of AVC and ASiCVC healed at 850 °C for 10 and 100 h, respectively as an example of surface degradations. First, fracture surface observations were conducted to identify

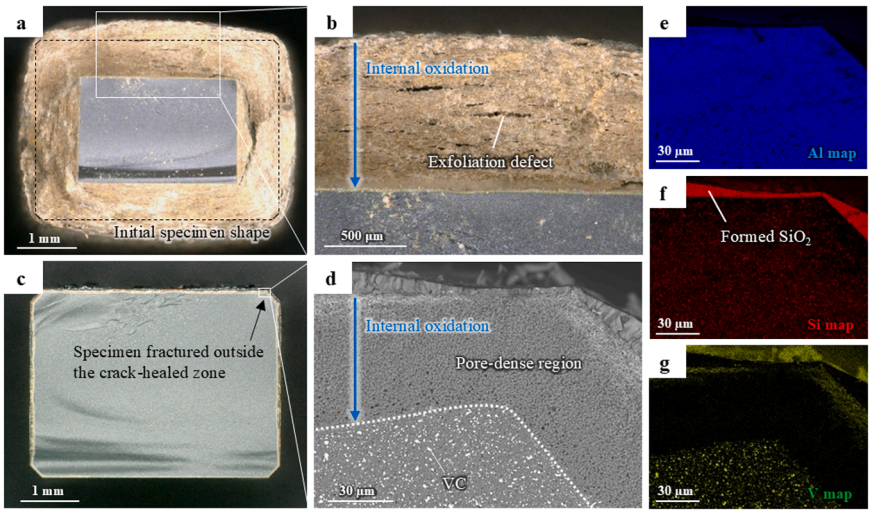

Fig. 6. Degradation behavior in AVC and ASiCVC. (a, b) Photomicroscope images of fractured surfaces in AVC (healing condition: 850 ℃ for 10 h). (c, d) Photomicroscope and backscattered electron images of fracture surfaces in ASiCVC (healing condition: 850 ℃ for 100 h). (e–g) Mapping images corresponding to panel (d).

the factors contributing to their degradation. Note that the healing temperature and time of AVC here is higher and much longer than those of the sample for structural analysis in Fig. 4, resulting in much thicker oxidation layer (approximately 1000 μm), to clarify the degradation behavior. These samples exhibited clear evidence of strength degradation and fractured outside the crack-healed zone (Fig. 1**g**).

In the case of AVC, the specimen exhibited oxidation-induced expansion, deviating from its initial shape, with the orange-colored oxide layer exceeding 1000 μm (Fig. 6a). Numerous exfoliation defects were observed within the oxidation layer of AVC (Fig. 6b). It is evident that excessive oxidation of the internal VC contributes to the formation of the degradation layer, as monolithic Al_2O_3 does not exhibit such volume expansion even after long-term heat treatment.

In the case of ASiCVC, no significant oxidation-induced expansion, as observed in AVC, was detected; however, internal oxidation with a thickness of several tens of micrometers was confirmed (Fig. 6c). In the enlarged SEM image at the fracture initiation site (Fig. 6c), numerous pores were observed within the internal oxidation layer (Fig. 6d). EDS mapping indicated that this pore-dense region coincided with the area where VC particles were consumed (Fig. 6e–g). Therefore, the formation of a pore-dense region beneath the surface, caused by the internal oxidation of VC and outward diffusion of V through grain boundaries, leads to significant strength degradation. Unlike AVC, a SiO_2 protective layer, ranging from several microns to several tens of microns in thickness, formed on the bulk surface (Fig. 6f).

Fig. 7a and b show the dependence of the depth of internal VC oxidation and strength degradation, respectively, on the heat-treatment time for AVC and ASiCVC. The internal oxidation depth was measured as the average of the measurements taken at three locations: both edges and the center of the fracture surface. In all samples, the internal oxidation depth increased as the heat-treatment time. Furthermore, higher heat-treatment temperatures led to greater propagation of internal oxidation. Notably, the increase in the internal oxidation depth in ASiCVC was several tens of times smaller than that in AVC, indicating that the addition of SiC effectively suppresses excessive internal oxidation.

As an additional experiment on strength degradation, the three-point bending strength of smooth specimens of AVC and ASiCVC heat-treated at 850–1000 °C for 10 min to 100 h was investigated (Fig. 7b). It was confirmed that the strength of both AVC and ASiCVC decreased with increasing heat-treatment time. Moreover, the decrease in the strength of AVC was much greater than that for ASiCVC. These results indicate a clear inverse correlation between strength degradation and the increase in the internal oxidation depth (Fig. 7a). Moreover, compared with the results shown in Fig. 1g, the strength of the crack-healed sample did not exceed that of the smooth-healed sample (Fig. 7c), indicating that degradation limited strength recovery. In addition, the degradation of ASiCVC was more gradual than that of AVC, highlighting that the addition of SiC is effective in preventing strength degradation during long-term oxidation.

From the above, it is evident that the formation and growth of the pore-dense layer caused by excessive oxidation of internal VC contributes to strength degradation, thereby hindering full-strength recovery. Furthermore, observations of the area around the healed crack in 3.3 indicate that the pores along both the bulk surface and crack pass represent the initial degradation caused by internal VC oxidation (Fig. 4a and Fig. 5a). This suggests that self-healing and degradation progress simultaneously during high-temperature oxidation. Furthermore, it can be concluded that the formation of a SiO_2 protective layer, resulting from the addition of SiC as a healing agent, is beneficial for preventing strength degradation by limiting the depth of the pore-dense region. The detail kinetic model for oxidation and degradation will be discussed in later 4.2.

4. Discussion

4.1. Self-healing mechanism by VC and SiC

The strength-recovery behavior and STEM observations clearly demonstrate that the simultaneous addition of VC and SiC healing agents to alumina decreased in the required healing time for reaching the strength of 500 MPa approximately 1/6000 times shorter compared with the addition of SiC alone. However, the incorporation of submicron- to micron-sized VC also led to dense pore formation and consequent strength degradation. Here, we summarize the oxidation-induced self-healing mechanism of VC and SiC healing agents, as well as the degradation mechanism, mainly resulting from VC oxidation. The accelerated healing mechanism can be explained based on the proposed healing process, which occurs through inflammation, repair, and remodeling stages [12].

Fig. 8 shows the crack-healing and degradation behaviors of ASiCVC. To assist in the discussion, a phase diagram calculated using FactSage is presented in Fig. 9. During the inflammation stage, external oxygen penetrates the crack-gap (Fig. 8a) and first oxidizes VC on the crack surfaces, resulting in the formation of V_2O_5 (l) above 700 °C as a healing agent (Fig. 8b). Furthermore, the reaction of V_2O_5 (l) with the matrix

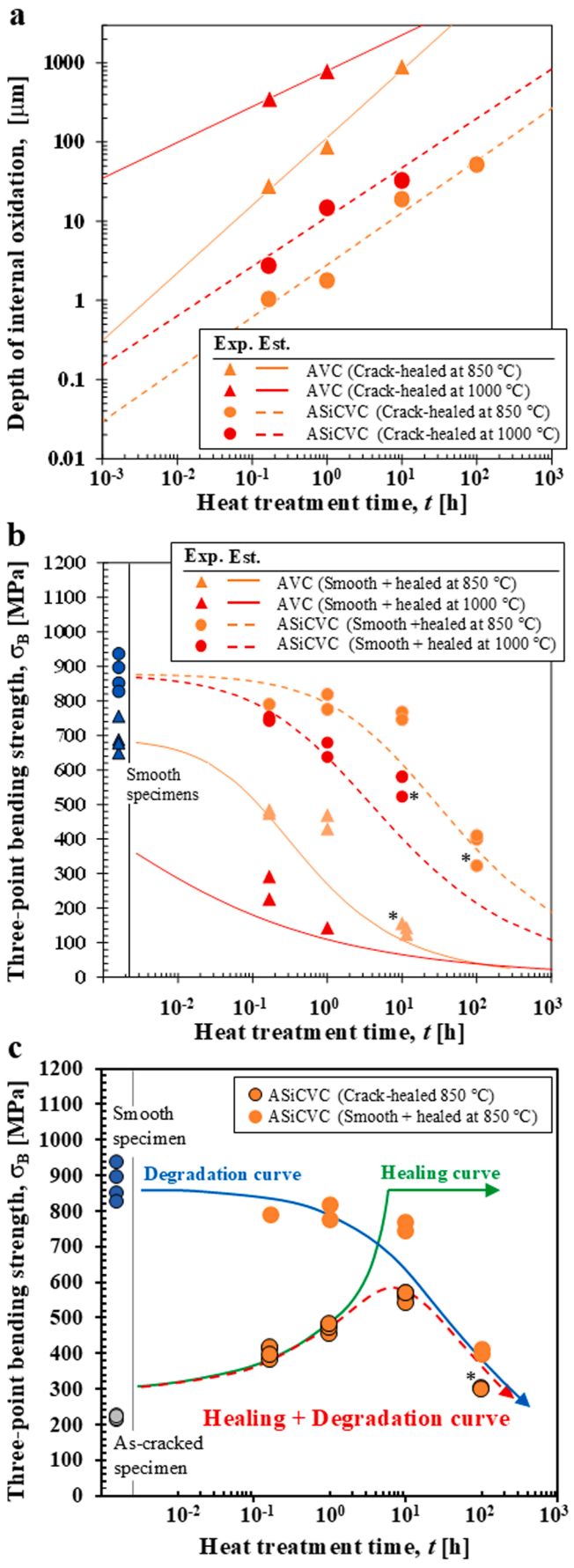

(caption on next column)

Fig. 7. Relationship between the heat treatment time and deterioration behavior in AVC and ASiCVC. (a) Relationship between the healing time and depth of internal oxidation in AVC and ASiCVC. (b) Relationship between the heat treatment time and three-point bending strength of smooth specimens. Here, * indicates the crack-healed specimen fracture from internal oxidation layer other than pre-crack shown in Fig. 1**g**. (c) Schematic illustration for healing and degradation behaviors in ASiCVC during 850 ℃ heat treatment.

forms V–Al–O melts with a V_2O_5:Al_2O_3 composition of approximately 95:5, which can be represented by a blue triangle in Figs. 9a and 9b. The compositions confirmed by the STEM with EDS analysis of AVC (Fig. 4h, Table 1). Therefore, under heat-treatment conditions of 700 °C or higher in air, the V_2O_5-containing Al in ASiCVC reaches its melting point and effectively fills the crack-gap and bulk surface (Fig. 8a and b). When the V–Al–O melts come into contact with SiC, they significantly accelerate the oxidation of the surrounding SiC, acting as a healing activator with an oxidizer, as described in 1 (Fig. 8c). The role of V_2O_5 (l) as an oxidizer of SiC during the inflammation stage is also demonstrated by the significant acceleration of the strength-recovery rate in alumina/SiC composites upon VC addition, as shown in Fig. 1g.

During the repair stage, supercooled melts of Si–V–Al–O with SiO_2-rich compositions are formed, and these low-viscosity supercooled melts rapidly fill the crack-gap (Fig. 8**d**), similar to the behavior observed with MnO [12]. As the oxidation of the internal VC progresses, V continuously diffuses along the grain boundaries. It is important to note that the formed Si–V–Al–O constitutes a SiO_2-rich glass phase with a higher melting point than that of the V_2O_5 single phase, as shown in Fig. 9**c**, despite VC oxidation being the initial self-healing reaction in ASiCVC. EDS analysis of areas 1–3 in Fig. 5**i** revealed that the converted SiO_2:V_2O_5:Al_2O_3 mole ratios in the Si-rich matrix phase and V-rich fine precipitates were approximately 97:2:1 and 86:13:1, respectively (Table 2). Although there is the limitations of the measurement accuracy in STEM-EDS using thin-film samples, the mole ratio of SiO_2:V_2O_5:Al_2O_3 in the supercooled melts before crystallization could be estimated at least between 96:2:1 and 86:13:1, because EDS results of the healed regions in both AVC and ASiCVC showed that the EDS compositions of alumina matrix phase were very close to the stoichiometric ratio of Al:O = 2:3 (Table 1, Table 2). Further, the volume fraction of V-rich fine precipitates in the Si-rich matrix phase was approximately 30 vol%, indicating that the mole ratio of SiO_2:V_2O_5:Al_2O_3 in the supercooled melts could be estimated as 94:5:1 by rule of mixtures. This composition is represented by a blue circle in Figs. 9**a** and 9**c**. Although the melting point of the Si–V–Al–O healing material is approximately 1650 °C, as indicated by the red solid line in Fig. 9**c**, the T_g estimated using the empirical rules reported by Osada [12] is 950 °C by the two-thirds rule and 650 °C by the one-half rule, as shown by the red dotted line in Fig. 9**c**. This implies that the formed V_2O_5 accelerates the repair stage, acting as a "healing activator with a viscosity modifier."

Finally, during the remodeling stage, the Si–V–Al–O supercooled melts undergo crystallization with two-phase separation into V- and Si-rich phases, resulting in the bonding of the crack surfaces (Figs. 8**e** and 8**f**). However, owing to the limitations of the measurement accuracy in STEM-EDS using thin-film samples, it was difficult to determine whether phase separation and crystallization of the supercooled melts occur during heating or cooling.

Equilibrium calculations using FactSage indicate that the SiO_2–5 mol % V_2O_5–1 mol% Al_2O_3 system at 1000 °C (represented by the blue circle in Fig. 9**c**) consists of approximately 80% solid SiO_2, which forms cristobalite, and 20% slag. During cooling and crystallization in this state, the V-rich phase precipitates only from the slag region, leading to variations in the distribution of V-rich precipitate particles within the healing area. However, no significant variation in the distribution of V-rich precipitate particles is observed (Fig. 5**i**), suggesting that most of the supercooled liquid in the healing area did not crystallize at 1000 °C but instead underwent two-phase separation into SiO_2 and V_2O_5 below the T_g during cooling. Nevertheless, with prolonged heating, the

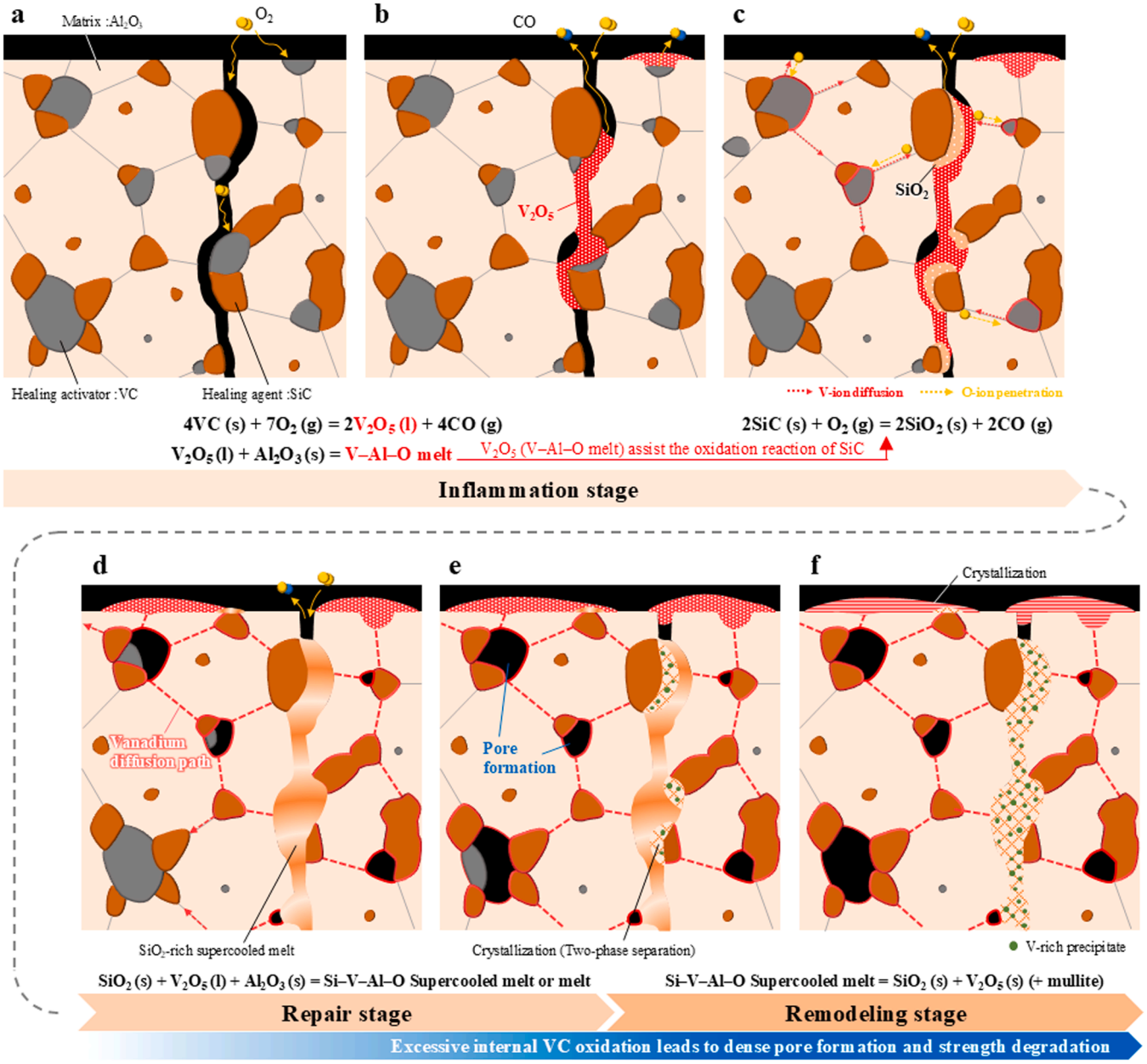

Fig. 8. Schematic illustration of the self-healing mechanism through the inflammation, repair, and remodeling stages, and the degradation mechanisms of alumina pre-incorporated with SiC and VC particles. (a) External oxygen penetrates the cracked surface and oxidizes SiC and VC. (b) Formed-V_2O_5 effectively diffuses into the crack-gap and bulk surface during liquefaction. (c) V_2O_5 assists with the oxidation reaction of SiC, and external oxygen penetration continues the internal VC oxidation. (d) A mechanically weak, low viscosity Si-V-Al-O supercooled melt or melt rapidly fills the crack-gap, resulting in the lowered the grass-transition temperature of healing material. (e) Mechanically strong crystals nucleate and grow in the supercooled melt with two-phase separation, forming V-rich precipitates and a Si-rich matrix phase. (f) Dense pore formation leads to degradation and undermining full-strength recovery.

preferential precipitation of solid SiO_2 may occur during high-temperature holding.

A high-temperature mechanical test is required in future studies to clarify the remodeling reaction and evaluate the strength of the healing material at the healing temperatures. Further, evaluating high-temperature strength between 400 and 800 °C range, which corresponds to bearing operating conditions, is critically important. However, because we could not propose a self-healing ceramic that fully restores the strength in this study, high-temperature strength testing does not be conducted. As a future work, optimization of particle size and volume fraction of the VC should be required based on the findings here regarding to self-healing and degradation, and then high-temperature strength evaluations would be performed.

4.2. Degradation behavior of Al_2O_3-containing VC particles

Fig. 8 shows the degradation behavior caused by excessive internal VC oxidation. During short- to middle-term heat treatment, oxygen-ion diffusion along the alumina grain boundaries to VC occurs owing to the gradient of oxygen partial pressure, leading to excessive internal VC oxidation (Fig. 8c–e). This internal oxidation promotes pore formation corresponding to the initial VC size, resulting in unexpected strength degradation. Even if long-term heat treatment moderately heals the crack, pore formation caused by deeper internal VC oxidation extends beyond the pre-crack, undermining full-strength recovery (Fig. 8f). The addition of SiC effectively suppresses the degradation caused by internal VC oxidation (Figs. 3, 6, and 7). However, because pore formation

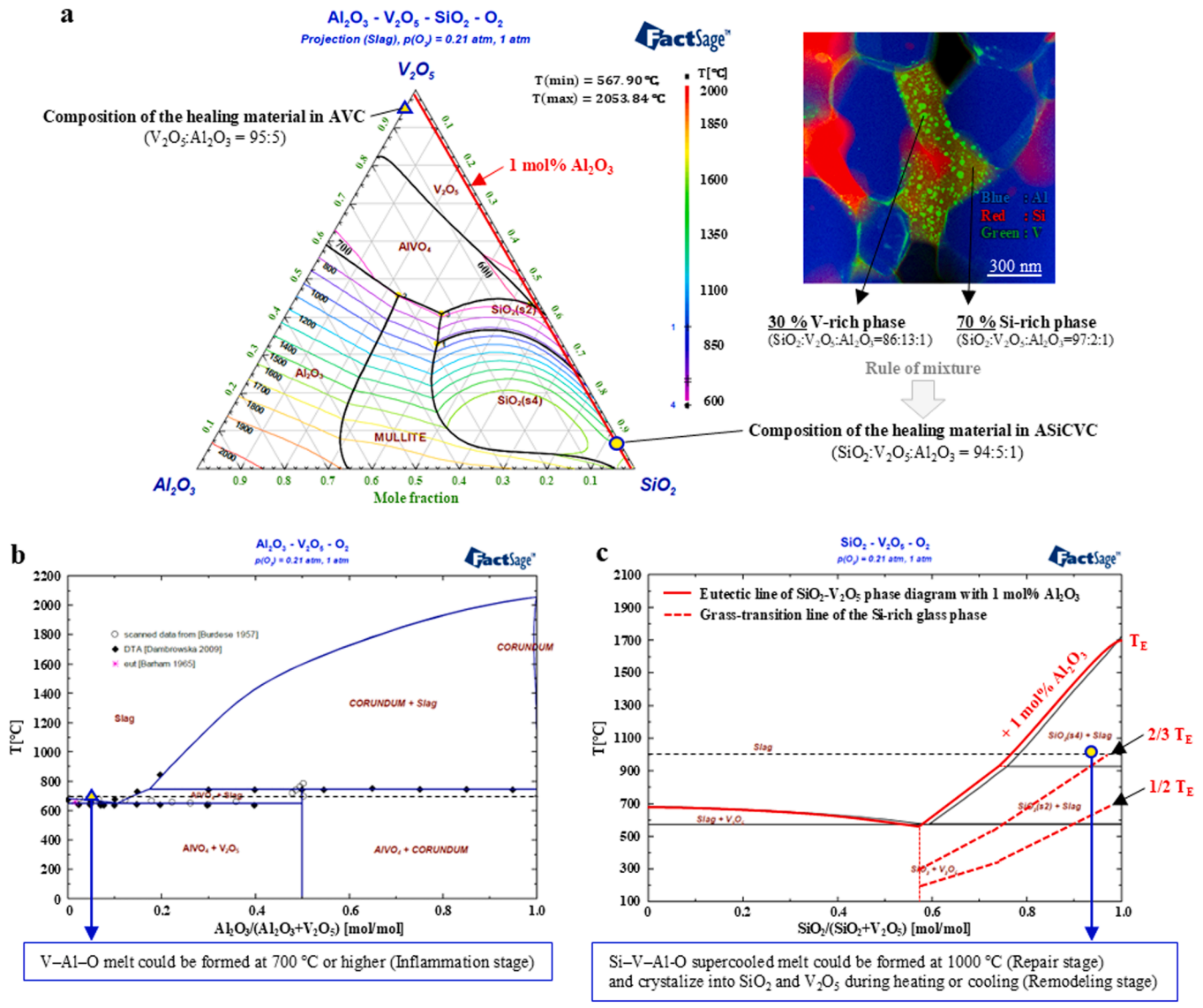

Fig. 9. Phase diagrams calculated using thermodynamic equilibrium software (FactSage): (a) Al_2O_3–V_2O_5–SiO_2, (b) Al_2O_3–V_2O_5, and (c) SiO_2–V_2O_5 systems.

within the VC particles cannot be completely avoided, practical application in turbine bearings that operate at high temperatures for extended periods may be challenging.

Here we propose a simple kinetic model for degradation behavior due to internal oxidation. The general form of depth gain of oxidation layer for isothermal oxidation at high temperature in air is given by

$$W = (k_p t)^{\frac{1}{n}} \tag{2}$$

where k_p is a rate constant, t is the heat treatment time. Meanwhile, n indicates the rate-controlling oxidation mechanism, and $n = 1$ and $n = 2$ corresponds to the values for reaction- and diffusion-controlled oxidation. From the analysis of experimental data in Fig. 7a based on the Eq. (2); n-value of AVC at 850 °C and 1000 °C were $n = 1.17$ and $n = 2.21$ respectively; n-value of ASiCVC at 850 °C and 1000 °C were $n = 1.52$ and $n = 1.69$ respectively. For healing due to SiC oxidation, $n = 2$ has been reported, indicating that Wagner's parabolic gain model controlling the diffusion within the SiO_2 protective layer is appropriate [15]. For composites with VC particles, the n-values lie between 1 and 2 except for the AVC at 1000 °C, implying that the oxide layer with dense-pores region corresponding to the initial VC size distribution is not protective as a diffusion path. The obtained constants including k_p are also summarized in Table 3. By imputing parameters into Eq. (3), the depth of oxidation layer W can be shown in Fig. 7a as a solid and dotted lines for AVC and ASiCVC, respectively.

Furthermore, the bending strength of specimens with the internal oxidation layer may be predicted by the final geometry of crack that propagates between large pores within the internal oxidation layer just before fracture during bending tests. Because the densely distributed pores act as stress concentration parts, crack may easily initiate at the largest pore and propagate at least to depth of internal oxidation layer before fracture. Therefore, simply assuming that the crack depth just before fracture is equivalent to the oxide layer depth, it is possible to predict the strength degradation behavior. The bending strength, σ_B, of ceramics can be estimated based on nonlinear elastic fracture mechanics according to process-zone size criteria as follows [15,40]:

Table 3
Kinetic parameters of internal oxidation for AVC and ASiCVC.

Materials	Temperature [°C]	k_P	n
AVC	850	7.05×10^{-2}	1.17
	1000	7.14×10^{2}	2.21
ASiCVC	850	1.33×10^{-3}	1.52
	1000	1.36×10^{-2}	1.69

$$\sigma_B = \text{Acos}\left\{\frac{8F^2c\sigma_o^2}{\pi K_{IC}^2 + 8F^2c\sigma_o^2}\right\}\frac{2\sigma_o}{\pi} \quad (3)$$

where c is the final depth of crack within internal oxidation layer; K_{IC} is the fracture toughness of composite; σ_o is the bending strength of smooth specimen without surface crack; F is the geometric factor of crack. By substituting Eq. (2) into Eq. (3), thus, the kinetic model for degradation behavior due to internal oxidation can be given by

$$\sigma_B = \text{Acos}\left\{\frac{8F^2(k_p t)^{\frac{1}{n}}\sigma_o^2}{\pi K_{IC}^2 + 8F^2(k_p t)^{\frac{1}{n}}\sigma_o^2}\right\}\frac{2\sigma_o}{\pi} \quad (4)$$

Here, we used $K_{IC} = 4.0$ MPa·m$^{0.5}$ for both composites which are the same values as Al_2O_3-30 vol% SiC composites [15]. Meanwhile, average values of σ_o of smooth specimens were used for prediction: σ_o= 692 MPa and σ_o= 879 MPa for AVC and ASiCVC, respectively. Although it is difficult to determine the F values for final geometry of crack with complicated shape, here we assume that final geometry of crack is semi-elliptical surface crack as the simplest assumption. Thus, $F = 0.72$ were used for estimation and can be calculated using the Newman– Raju equation [41]

In Fig. 7b, the lines estimated for AVC and ASiCVC heat-treated at 850 °C and 1000 °C, respectively, were shown for the comparison with experimental bending strength. Estimated lines by proposed kinetic model for degradation show in good agreement with experimental degradation behavior under all the tested conditions, although the model involved some assumptions. Thus, we can conclude that the degradation of strength results from formation of densely distributed pores by internal oxidation of VC particles and from formation of large crack due to the connection of pores within the internal oxidation layer just before fracture during bending tests.

As an analogous example of degradation in self-healing ceramics, Wang et al. reported that in a SiC–Al_2O_3–B_4C system, the bending strength decreases with increasing the healing time, leading to pore formation and CO_2 gas generation due to excessive oxidation of pre-incorporated B_4C particles [42]. Since VC is oxidation-active and generate CO/CO_2 gas during oxidation, a similar degradation mechanism is likely to occur in the present system as well. Therefore, the structure of the VC additive must be redesigned so that the pores formed do not compromise the strength, considering both their size and proportion.

5. Conclusions

This study developed Al_2O_3-based ceramics incorporating VC particles for bearing applications. Two composite types, AVC and ASiCVC, were prepared and their self-healing behaviors were investigated. AVC achieved a maximum strength recovery of 313 MPa at 850 °C for 10 min, while ASiCVC reached 674 MPa at 1000 °C for 10 min, indicating that the required healing time for reaching the strength of 500 MPa in ASiCVC was 1/6000 times shorter than that in Al_2O_3-SiC composites without VC addition. The formed V_2O_5 showed limited contribution to strength recovery owing to its weak interlayer structure, indicating that VC alone has limited potential as a healing agent. However, the formed V_2O_5 effectively diffused into crack-gaps and along alumina grain boundaries, resulting in lowered the T_g of SiO_2–Al_2O_3-based healing materials, demonstrating that VC possesses promising potential as a healing activator. Excessive oxidation of internal VC created pores and led to unexpected matrix degradation, while the addition of SiC suppressed the propagation of internal oxidation.

CRediT authorship contribution statement

Taro Oshiumi: Writing – original draft, Visualization, Methodology, Investigation, Data curation, Conceptualization. **Toru Hara:** Writing – review & editing, Resources, Investigation. **Masahiro Goto:** Writing – review & editing, Resources. **Toshio Osada:** Writing – review & editing, Supervision, Conceptualization, Resources.

Declaration of Generative AI and AI-assisted technologies in the writing process

During the preparation of this work the first author used Azure GPT-4o in order to improve readability of the text. After using this tool/service, the author(s) reviewed and edited the content as needed and take(s) full responsibility for the content of the published article.

Funding

This research did not receive any specific grant from funding agencies in the public, commercial, or not-for-profit sectors.

Declaration of Competing Interest

There are no conflicts of interest to declare.

Acknowledgements

Acknowledgments are extended to Ms. Yuka Hara and Ms. Akiko Nakamura of NIMS for their assistance with FIB-SEM analysis. The authors also thank Akifumi Takeuchi and Takashi Nogawa of same department at PROTERIAL for their technical advice. English editing was provided by Editage (www.editage.jp).

References

[1] E.V. Zaretsky, Y.P. Chiu, T.E. Tallian, Ceramic bearings for use in gas turbine engines, J. Mater. Eng. 11 (1989) 237–253, https://doi.org/10.1007/BF02834841.
[2] F.D. Slaney, Hybrid ceramic bearing development for gas turbine engines, in: Power for Land, Sea, and Air, American Society of Mechanical Engineers, The Hague, 1994, https://doi.org/10.1115/94-GT-112.
[3] M. Kitamura, Trends and future views on rolling bearing technology, JTEKT Eng. J. 1003 (2007) 9–16.
[4] A.A. Griffith, The phenomena of rupture and flow in solids, Philos. Trans. R. Soc. A 221 (1921) 163–198, https://doi.org/10.1098/rsta.1921.0006.
[5] G.H.Von Fuchs, H. Diamond, Oxidation characteristics of lubricating oils, Ind. Eng. Chem. 34 (1942) 927–937, https://doi.org/10.1021/ie50392a007.
[6] M. Sarkar, N. Mandal, Solid lubricant materials for high temperature application: a review, Mater. Today Proc. 66 (2022) 3762–3768, https://doi.org/10.1016/j.matpr.2022.06.030.
[7] M.C. Chu, S. Sato, Y. Kobayashi, K. Ando, Damage healing and strengthening behavior in intelligent mullite-sic ceramics, Fatigue Fract. Eng. Mater. Struct. 18 (1995) 1019–1029, https://doi.org/10.1111/j.1460-2695.1995.tb00924.x.
[8] B.S. Kim, K. Ando, M.C. Chu, S. Saito, Crack-healing behavior of monolithic alumina and strength of crack-healed member, Zairyo 52 (2003) 667–673.
[9] K. Takahashi, M. Yokouchi, S.K. Lee, K. Ando, Crack-healing behavior of Al_2O_3 toughened by SiC whiskers, J. Am. Ceram. Soc. 86 (2003) 2143–2147, https://doi.org/10.1111/j.1151-2916.2003.tb03622.x.
[10] K. Ando, B.S. Kim, M.C. Chu, S. Saito, K. Takahashi, Crack-healing and mechanical behaviour of Al_2O_3-SiC composites at elevated temperature, Fatigue Fract. Eng. Mater. Struct. 27 (2004) 533–541, https://doi.org/10.1111/j.1460-2695.2004.00785.x.
[11] T. Osada, W. Nakao, K. Takahashi, K. Ando, Kinetics of self-crack-healing of alumina-silicon carbide composite including oxygen partial pressure effect, J. Am. Ceram. Soc. 92 (2009) 864–869, https://doi.org/10.1111/j.1551-2916.2009.02992.x.
[12] T. Osada, K. Kamoda, M. Mitome, T. Hara, T. Abe, Y. Tamagawa, W. Nakao, T. Ohmura, A novel design approach for self-crack-healing structural ceramics with 3D networks of healing activator, Sci. Rep. 7 (2017) 17853, https://doi.org/10.1038/s41598-017-17942-6.
[13] Y. Oba, K. Takeo, W. Nakao, S. Ozaki, Numerical study on crack bifurcation of self-healing fiber-reinforced ceramic matrix composite, Mech. Eng. J. 4 (2017) 16-00705, https://doi.org/10.1299/mej.16-00705.
[14] W. Nakao, T. Hayakawa, T. Yanaseko, S. Ozaki, Advanced fiber reinforced self-healing ceramics for middle range temperature, Key Eng. Mater. 810 (2019) 119–124, https://doi.org/10.4028/www.scientific.net/KEM.810.119.
[15] T. Osada, T. Hara, M. Mitome, S. Ozaki, T. Abe, K. Kamoda, T. Ohmura, Self-healing by design: universal kinetic model of strength recovery in self-healing ceramics, Sci. Technol. Adv. Mater. 21 (2020) 593–608, https://doi.org/10.1080/14686996.2020.1796468.

[16] S. Ozaki, M. Nakamura, T. Osada, Finite element analysis of the fracture statistics of self-healing ceramics, Sci. Technol. Adv. Mater. 21 (2020) 609–625, https://doi.org/10.1080/14686996.2020.1800368.
[17] T. Maeda, T. Osada, S. Ozaki, Novel numerical approach for reliability-assurance of ceramics by combining self-crack-healing with proof testing, J. Eur. Ceram. Soc. 44 (2024) 2261–2270, https://doi.org/10.1016/j.jeurceramsoc.2023.10.077.
[18] S. Yoshioka, L. Boatemaa, S. van der Zwaag, W. Nakao, W.G. Sloof, On the use of TiC as high-temperature healing particles in alumina based composites, J. Eur. Ceram. Soc. 36 (2016) 4155–4162, https://doi.org/10.1016/j.jeurceramsoc.2016.06.008.
[19] L. Boatemaa, S. van der Zwaag, W.G. Sloof, Self-healing of Al_2O_3 containing Ti microparticles, J. Ceram. Int. 44 (2018) 11116–11126, https://doi.org/10.1016/j.ceramint.2018.03.119.
[20] Z. Chen, L. Ji, N. Guo, C. Xu, S. Zhang, Crack healing and strength recovery of Al_2O_3/TiC/TiB_2 ceramic tool materials, Int. J. Refract. Met. Hard Mater. 87 (2020) 105167, https://doi.org/10.1016/j.ijrmhm.2019.105167.
[21] S.T. Nguyen, A. Okawa, M.D. Thi, C.M. Ngo, T. Takahashi, T. Nakayama, H. Suematsu, K. Niihara, Self-healing ability and full strength recovery at medium temperatures of low content titanium carbide/alumina composites, J. Ceram. Soc. Jpn. 132 (2024) 85–92, https://doi.org/10.2109/jcersj2.23176.
[22] S. Yoshioka, W. Nakao, Methodology for evaluating self-healing agent of structural ceramics, J. Intell. Mater. Syst. Struct. 26 (2015) 1395–1403, https://doi.org/10.1177/1045389X14544137.
[23] S. Li, G. Song, K. Kwakernaak, S. van der Zwaag, W.G. Sloof, Multiple crack healing of a Ti_2AlC ceramic, J. Eur. Ceram. Soc. 32 (2012) 1813–1820, https://doi.org/10.1016/j.jeurceramsoc.2012.01.017.
[24] S. Li, G. Bei, X. Chen, L. Zhang, Y. Zhou, M. Mačković, E. Spiecker, P. Greil, Crack healing induced electrical and mechanical properties recovery in a Ti_2SnC ceramic, J. Eur. Ceram. Soc. 36 (2016) 25–32, https://doi.org/10.1016/j.jeurceramsoc.2015.09.019.
[25] Z. Wang, J. Sun, B. Xu, Y. Liu, P. Ke, A. Wang, Reducing the self-healing temperature of Ti_2AlC MAX phase coating by substituting Al with Sn, J. Eur. Ceram. Soc. 40 (2020) 197–201, https://doi.org/10.1016/j.jeurceramsoc.2019.09.009.
[26] M. El Laithy, L. Wang, T.J. Harvey, B. Vierneusel, M. Correns, T. Blass, Further understanding of rolling contact fatigue in rolling element bearings - a review, Tribol. Int. 140 (2019) 105849, https://doi.org/10.1016/j.triboint.2019.105849.
[27] X. Zhang, D. Wu, Z. Xia, Y. Li, J. Wang, E.H. Han, Characteristics and mechanism of surface damage of hybrid ceramics ball bearings for high-precision machine tool, Eng. Fail Anal. 142 (2022) 106784, https://doi.org/10.1016/j.engfailanal.2022.106784.
[28] S. Shi, T. Goto, S. Cho, T. Sekino, Electrochemically assisted room-temperature crack healing of ceramic-based composites, J. Am. Ceram. Soc. 102 (2019) 4236–4246, https://doi.org/10.1111/jace.16264.
[29] K. Morita, F. Naito, D. Terada, Microcrack healing in zirconia ceramics under a DC electric field/current, J. Eur. Ceram. Soc. 41 (2021) 282–289, https://doi.org/10.1016/j.jeurceramsoc.2021.09.044.
[30] C. Santafé, C. Borgianni, Study of the oxidation kinetics of vanadium carbide, Oxid. Met. 9 (1975) 415–425, https://doi.org/10.1007/BF00611690.
[31] J. Matsushita, T. Nakayama, Oxidation behavior of vanadium carbide powder, J. Adv. Sci. 10 (1998) 97–99, https://doi.org/10.2978/jsas.10.2-3_97.
[32] H. Suzuki, Effect of vanadium oxide on the oxidation of silicon carbide, Ceram. Assoc. Jpn. 68 (1960) 220–221, https://doi.org/10.2109/jcersj1950.68.777_210.
[33] J.B. Goodenough, Metallic oxides, Prog. Solid State Chem. 5 (1971) 145–399, https://doi.org/10.1016/0079-6786(71)90018-5.
[34] H. Chacon-Tribin, J. Loftus, C.N. Satterfield, Viscosity of the vanadium pentoxide-potassium sulfate eutectic, J. Chem. Eng. Data 11 (1966) 44–45, https://doi.org/10.1021/je60028a010.
[35] E. Lugscheider, S. Bärwulf, C. Barimani, Properties of tungsten and vanadium oxides deposited by MSIP-PVD process for self-lubricating applications, Surf. Coat. Technol. 120–121 (1999) 458–464, https://doi.org/10.1016/S0257-8972(99)00467-3.
[36] A. Erdemir, A crystal chemical approach to the formulation of self-lubricating nanocomposite coatings, Surf. Coat. Technol. 200 (2005) 1792–1796, https://doi.org/10.1016/j.surfcoat.2005.08.054.
[37] R. Franz, C. Mitterer, Vanadium containing self-adaptive low-friction hard coatings for high-temperature applications: a review, Surf. Coat. Technol. 228 (2013) 1–13, https://doi.org/10.1016/j.surfcoat.2013.04.034.
[38] K. Broniszewski, J. Wozniak, M. Kostecki, K. Czechowski, L. Jaworska, A. Olszyna, Al_2O_3–V cutting tools for machining hardened stainless steel, Ceram. Int. 41 (2015) 14190–14196, https://doi.org/10.1016/j.ceramint.2015.07.044.
[39] J.S. Association, Testing method for flexural strength of fine ceramics at room temperature, J. Ind. Stand. (2008).
[40] K. Ando, Y. Shirai, M. Nakatani, Y. Kobayashi, S. Sato, Crack-healing + proof test): a new methodology to guarantee the structural integrity of a ceramics component, J. Eur. Ceram. Soc. 22 (2002) 121–128, https://doi.org/10.1016/S0955-2219(01)00236-9.
[41] J.C. Newman Jr., I.S. Raju, An empirical stress-intensity factor equation for surface crack, Eng. Fract. Mech. 15 (1981) 185–192, https://doi.org/10.1016/0013-7944(81)90116-8.
[42] B. Wang, R. Tu, Y. Wei, H. Cai, Self-healing of SiC-Al_2O_3-B_4C ceramic composites at low temperatures, Materials 15 (2022) 652, https://doi.org/10.3390/ma15020652.